

Nonequilibrium Green's-function method applied to double-barrier resonant-tunneling diodes

Roger Lake and Supriyo Datta

School of Electrical Engineering, Purdue University, West Lafayette, Indiana 47907

(Received 15 July 1991; revised manuscript received 8 November 1991)

The effect of inelastic scattering on quantum electron transport through double-barrier resonant-tunneling structures with large cross-sectional areas is studied numerically using the approach based on the nonequilibrium Green's-function formalism of Keldysh, Kadanoff, and Baym. The Markov assumption is not made, and the energy coordinate is retained. This makes the inclusion of the phonon-energy spectrum straightforward both conceptually and in practice. The electron-phonon interaction is treated in the self-consistent first Born approximation (SCFBA). The Pauli exclusion principle is taken into account exactly within the SCFBA. The retention of the energy coordinate allows the calculation of a number of quantities that give insight into the effect of inelastic scattering on electron transport: The effect of inelastic scattering on the occupation of the energy levels, the density of states, the energy distribution of the current density, and the power density is calculated from a quantum kinetic equation for actual device structures under high bias.

I. INTRODUCTION

The treatment of inelastic scattering in quantum transport is interesting from both a theoretical and a practical point of view. From a practical perspective, the success of the technology of molecular-beam epitaxy has allowed the fabrication of layered semiconductor structures such as double-barrier resonant-tunneling diodes (DBRTD's),¹ superlattices,² and hot-electron injection devices³ which operate on quantum mechanical principles under high bias. If one wishes to describe experiments on these structures, such as photoluminescence measurements of the occupation of resonant levels,⁴ or the valley current of a DBRTD,⁵ a treatment of inelastic scattering is necessary.

Theoretically, there have been many studies of the effect of inelastic scattering on resonant tunneling.⁶⁻¹⁴ The treatment of the elastic and inelastic scattering ranges in various degrees of sophistication. As discussed by Pevzner, Sols, and Hess¹⁵ and Sols,¹⁶ it is relatively easy to treat coherent elastic scattering from potential barriers and device geometries exactly using numerical methods while the inelastic scattering is treated in an approximation. Two approximations are commonly used:⁸⁻¹² (1) the inelastic scattering is confined to a finite region of space, and (2) the inelastic scattering is treated within the one-electron picture, i.e., the Pauli exclusion principle is ignored.

The numerical approach that has been used to study the effect of inelastic scattering on DBRTD's has been based on a solution of the Wigner-Weyl transform of the Liouville equation for the Wigner function.¹⁷⁻²¹ The inclusion of inelastic scattering in the above work has been conceptually problematic.^{20,21} The exact forms for the self-energy terms have recently been derived from a Wigner-Weyl transformation of the general equations of Keldysh, Kadanoff, and Baym.²¹ However, in practice, a relaxation-time approximation is used.^{17-19,21}

The approach used in this work begins with the general many-body, non-equilibrium Green's-function theory of Keldysh, Kadanoff, and Baym,^{22,23} which we will refer to as the KKB formalism. It is restricted to steady state. The Pauli exclusion principle is rigorously included. Three approximations are made.

(i) Electron-phonon interaction is treated in the self-consistent first Born approximation, which means that only one-phonon scattering is included, but it is included exactly (to all orders in the language of perturbation theory).

(ii) The phonons are modeled as a bath of independent oscillators which interact with the electrons locally. This corresponds to a simple model of deformation potential dispersionless optical phonons with the potential felt by the electrons proportional to the ionic displacement.

(iii) The phonon coordinates are traced out by assuming that the phonons remain in equilibrium.

The phonons are not restricted to a finite region of space but extend throughout the device and contacts from $-\infty$ to $+\infty$ in the case of a 1D (Ref. 24) simulation.

The fundamental quantity in the KKB formalism is the two-time correlation function, $G^<(\mathbf{r}_1, t_1; \mathbf{r}_2, t_2)$. By performing a Wigner transform on the time variables, we can write the correlation function as $G^<(\mathbf{r}_1, \mathbf{r}_2; E, T)$, where $T = \frac{1}{2}(t_1 + t_2)$ and E/\hbar is the Fourier transform variable corresponding to the time difference coordinate $(t_1 - t_2)$. The fundamental quantity in the Liouville equation, the density matrix $\rho(\mathbf{r}_1, \mathbf{r}_2; T)$, is obtained by setting $t_1 = t_2$ in $G^<$, which is equivalent to integrating over energy, $\rho(\mathbf{r}_1, \mathbf{r}_2; T) = \int (dE/2\pi) G^<(\mathbf{r}, \mathbf{r}'; E, T)$.^{20,25}

The KKB formalism gives energy resolved information. The retention of the energy coordinate makes the inclusion of the phonon energy spectrum straightforward both conceptually and in practice. It also allows the calculation of a number of quantities which give insight into the effect of inelastic scattering on quantum electron

transport. The effect of transitions between levels can be seen in the occupation of energy levels and in the energy distribution of the current density. Knowing the mean energy of the current density, the spatial distribution of the power being dissipated by the electrons to the phonon bath can be calculated throughout the device. Numerical examples of all the above-mentioned quantities will be presented in this paper.

II. STEADY-STATE KKB FORMALISM

There has been much work based on the KKB formalism and there have been several excellent reviews (see Ref. [26–28] and references therein). Our concern is with steady-state transport in mesoscopic systems. In steady state, the coupled nonequilibrium Green's function equations take on a relatively simple form which provides a good starting point for a general, quantum-mechanical treatment of electron-phonon and electron-electron interactions in mesoscopic structures far from equilibrium. We summarize below a steady-state version of the KKB formalism that is the starting point of this work.

We do not make the gradient expansion²⁸ since potentials in mesoscopic systems vary rapidly in space. In steady state, it is assumed that there is no dependence on the center-of-mass time $(t+t')/2$ and we Fourier transform the relative time coordinate to energy E . The notation and definitions for the Green's functions and self-energies correspond to that found in Ref. 29. The equations for the retarded Green's function G^R and the correlation functions $G^<$ are^{28–30}

$$[E - H_0(\mathbf{r})]G^R(\mathbf{r}, \mathbf{r}'; E) - \int d\mathbf{r}_1 \Sigma^R(\mathbf{r}, \mathbf{r}_1)G^R(\mathbf{r}_1, \mathbf{r}'; E) = \delta(\mathbf{r} - \mathbf{r}'), \quad (1)$$

$$G^<(\mathbf{r}, \mathbf{r}'; E) = \int d\mathbf{r}_1 d\mathbf{r}_2 G^R(\mathbf{r}, \mathbf{r}_1; E) \times \Sigma^<(\mathbf{r}_1, \mathbf{r}_2; E)G^R(\mathbf{r}_2, \mathbf{r}'; E). \quad (2)$$

Since we are only concerned with steady state, a boundary term has been dropped from (2) which depends on the time at which the interaction is adiabatically turned on.³⁰ We write the retarded self-energy Σ^R as

$$\Sigma^R(\mathbf{r}, \mathbf{r}'; E) = \sigma(\mathbf{r}, \mathbf{r}'; E) - \frac{i\Gamma(\mathbf{r}, \mathbf{r}'; E)}{2}, \quad (3)$$

where $\sigma = (\Sigma^R + \Sigma^A)/2$ and $-i\Gamma/2 = (\Sigma^R - \Sigma^A)/2$. In (3), σ is the Hermitian part of Σ^R , and $i\Gamma/2$ is the anti-Hermitian part of Σ^R . If we Fourier transform the relative coordinate $\mathbf{r} - \mathbf{r}'$ to \mathbf{k} , σ and $i\Gamma/2$ become, respectively, the real and imaginary parts of $\Sigma^R(\mathbf{R}, \mathbf{k}; E)$, where \mathbf{R} is the center-of-mass coordinate $(\mathbf{r} + \mathbf{r}')/2$.²⁶ The Hermitian part of Σ^R is the Hilbert transform of the anti-Hermitian part plus a term Σ_{HF} due to the singular part of Σ^R from the Hartree-Fock diagrams:²⁶

$$\sigma(\mathbf{r}, \mathbf{r}'; E) = \frac{1}{\pi} \mathcal{P} \int \frac{dE'}{2\pi} \frac{\Gamma(\mathbf{r}, \mathbf{r}'; E')}{E - E'} + \Sigma_{\text{HF}}. \quad (4)$$

Γ is given by the sum of the in-scattering function $\Sigma^<$ and the out-scattering function $\Sigma^>$:

$$\Gamma(\mathbf{r}, \mathbf{r}'; E) = -i(\Sigma^<(\mathbf{r}, \mathbf{r}'; E) - \Sigma^>(\mathbf{r}, \mathbf{r}'; E)). \quad (5)$$

$\Sigma^<$ depends on the type of interaction being considered. Once $\Sigma^<$ and $\Sigma^>$ are specified, (1)–(5) plus the equations for $\Sigma^<$ become the closed set of equations that need to be solved.

The systems we consider are those with boundary conditions (an applied bias) that have been fixed for a long time. However, there is some evidence from numerical simulations that such systems may not reach steady state³¹; Coulomb charging effects can result in high-frequency oscillations in the current for a fixed applied voltage. Under such circumstances, the steady-state equations cannot be used.

III. POINT SCATTERER MODEL

In this work (following Ref. 29) we use a model for which the in-scattering and out-scattering functions $\Sigma^<(\mathbf{r}, \mathbf{r}'; E)$ and $\Sigma^>(\mathbf{r}, \mathbf{r}'; E)$ are proportional to δ functions in space. This leads to a simplification of the transport equations as described in the following section. The physical model is described by the following three Hamiltonians.²⁹ The electrons are described by the one-electron effective-mass Hamiltonian

$$H_0 = \frac{(\mathbf{p} - e\mathbf{A})^2}{2m^*} + V(\mathbf{r}), \quad (6)$$

where V includes the linear potential drop and the conduction-band discontinuities. Magnetic fields are neglected in this work ($\mathbf{A} = 0$). Dephasing is assumed to be caused by a reservoir of independent oscillators (maintained in thermodynamic equilibrium) described by

$$H_B = \sum_m \hbar\omega_m (a_m^\dagger a_m + \frac{1}{2}). \quad (7)$$

The electrons are assumed to interact with the bath through a δ potential

$$H' = \sum_m U \delta(\mathbf{r} - \mathbf{r}_m) (a_m^\dagger + a_m). \quad (8)$$

Assuming a continuum of modes, the sum over m becomes an integral $\sum_m \rightarrow \int d\mathbf{r} \int d(\hbar\omega) J_0(\mathbf{r}; \hbar\omega)$, where J_0 is the density of oscillator modes. One is free to choose the energy spectrum $J_0(\hbar\omega)$ of the oscillators. In this work, we have used three different models.

(i) Elastic phase breaking: $J_0(\hbar\omega) \sim \delta(\omega)$.

(ii) Einstein phonon: $J_0(\hbar\omega) \sim \delta(\omega \pm \omega_0)$, $\hbar\omega_0 = 36$ meV.

(iii) Debye phonon: $J_0(\hbar\omega) \sim \omega^2 \Theta(\omega_D - |\omega|)$, $\hbar\omega_D = 20$ meV.

This allows comparisons between simple elastic phase breaking and inelastic scattering where transitions between energy levels are present. When we model inelastic scattering, both the Debye and Einstein oscillators are included. The Debye oscillators allow for small energy transitions and close the energy gap that would otherwise occur in Σ^R at low temperatures.³²

When the Einstein spectrum is used, the local oscillator model corresponds precisely to a simple model for dispersionless deformation potential optical phonons

(DPOP's). This is shown as follows. The potential felt by the electrons due to the phonons for DPOP's is

$$H_{\text{ep}}(\mathbf{r}, t) = \frac{1}{\sqrt{V}} M \sum_{\mathbf{q}} e^{i\mathbf{q}\cdot\mathbf{r}} (a_{\mathbf{q}} e^{-i\omega_{\mathbf{q}}t} + a_{-\mathbf{q}}^{\dagger} e^{i\omega_{\mathbf{q}}t}). \quad (9)$$

Then $D^{<} = \langle H_{\text{ep}}(\mathbf{r}, t) H_{\text{ep}}(\mathbf{r}', t') \rangle$ is²⁹

$$D^{<}(\mathbf{r}_1, \mathbf{r}_2; \hbar\omega) = M^2 (2\pi) \delta(\mathbf{r}_1 - \mathbf{r}_2) \times \{ |N(\omega_0) + 1| \delta(\omega + \omega_0) + N(\omega_0) \delta(\omega - \omega_0) \}, \quad (10)$$

where N is the Bose-Einstein factor. This is precisely the form of $D^{<}$ when using the Einstein spectrum in the local oscillator model [compare Eq. (A8a) in Ref. 29].

IV. STEADY-STATE KKB FORMALISM APPLIED TO POINT SCATTERERS

We introduce a few identities and one definition. We need the identities for the electron density per unit energy $n(\mathbf{r}; E) = (-i/2\pi) G^{<}(\mathbf{r}, \mathbf{r}; E)$ the hole density $p(\mathbf{r}; E) = (i/2\pi) G^{>}(\mathbf{r}, \mathbf{r}; E)$, and the local density of states $N_0(\mathbf{r}; E) = n(\mathbf{r}; E) + p(\mathbf{r}; E) = -1/\pi \text{Im} G^R(\mathbf{r}, \mathbf{r}; E)$. We define the nonequilibrium occupation factor as $f(\mathbf{r}; E) = n(\mathbf{r}; E)/N_0(\mathbf{r}; E)$. At equilibrium, $f(\mathbf{r}; E)$ is simply the Fermi-Dirac factor.

In this work, the self-energies for the electron-phonon interaction are evaluated in the self-consistent Born approximation,

$$\Sigma^{\lessgtr}(\mathbf{r}, \mathbf{r}'; E) = \int dE' G^{\lessgtr}(\mathbf{r}, \mathbf{r}'; E - E') D^{\lessgtr}(\mathbf{r}, \mathbf{r}'; E') \quad (11)$$

where

$$D^{\lessgtr}(\mathbf{r}, \mathbf{r}'; E) = \int d(t - t') e^{iE(t - t')/\hbar} \times \langle H'(\mathbf{r}, t) H'(\mathbf{r}', t') \rangle.$$

Since, in our model, the electron-phonon interaction is local, the corresponding self-energies, in the self-consistent first Born approximation (SCFBA), are local. We write the self-energies as

$$\Sigma^{<}(\mathbf{r}_1, \mathbf{r}_2; E) = -i \frac{\hbar}{\tau_p(\mathbf{r}_1; E)} \delta(\mathbf{r}_1 - \mathbf{r}_2),$$

$$\Sigma^{>}(\mathbf{r}_1, \mathbf{r}_2; E) = +i \frac{\hbar}{\tau_n(\mathbf{r}_1; E)} \delta(\mathbf{r}_1 - \mathbf{r}_2),$$

and

$$\Sigma^R(\mathbf{r}_1, \mathbf{r}_2; E) = \left[\sigma(\mathbf{r}_1; E) - i \frac{\hbar}{2\tau_{\phi}(\mathbf{r}_1; E)} \right] \delta(\mathbf{r}_1 - \mathbf{r}_2),$$

where $1/\tau_n$ is the electron outscattering rate, $1/\tau_p$ is the hole outscattering rate, $1/\tau_{\phi}$ is the total dephasing rate, and σ is the real part of Σ^R .

Only the diagonal elements of G^{\lessgtr} are needed to calculate the self-energies because of the local nature of the interaction. With the above identities and definitions, the coupled equations for G^R , the diagonal elements of $G^{<}$, Σ^{\lessgtr} , and Σ^R take the following forms, respectively:

$$\left[E - H_0(\mathbf{r}) - \sigma(\mathbf{r}; E) + i \frac{\hbar}{2\tau_{\phi}(\mathbf{r}; E)} \right] G^R(\mathbf{r}, \mathbf{r}'; E) = \delta(\mathbf{r} - \mathbf{r}'), \quad (12)$$

$$f(\mathbf{r}; E) = \frac{1}{N_0(\mathbf{r}; E)} \frac{\hbar}{2\pi} \int d\mathbf{r}' \frac{|G^R(\mathbf{r}, \mathbf{r}'; E)|^2}{\tau_p(\mathbf{r}'; E)}, \quad (13)$$

$$\frac{1}{\tau_p(\mathbf{r}; E)} = \frac{2\pi}{\hbar} \int d(\hbar\omega) F(\mathbf{r}, \hbar\omega) \times N_0(\mathbf{r}; E - \hbar\omega) f(\mathbf{r}; E - \hbar\omega), \quad (14a)$$

$$\frac{1}{\tau_n(\mathbf{r}; E)} = \frac{2\pi}{\hbar} \int d(\hbar\omega) F(\mathbf{r}, \hbar\omega) N_0(\mathbf{r}; E + \hbar\omega) \times [1 - f(\mathbf{r}; E + \hbar\omega)], \quad (14b)$$

$$\frac{1}{\tau_{\phi}(\mathbf{r}; E)} = \frac{1}{\tau_p(\mathbf{r}; E)} + \frac{1}{\tau_n(\mathbf{r}; E)}. \quad (15)$$

So far, in practice, we have ignored the real part of Σ^R . In (14), F is a known function consisting of a strength U , the density of oscillator modes J_0 , and the Bose-Einstein factor N :

$$F(\mathbf{r}, \hbar\omega) = U^2 J_0(\mathbf{r}, |\omega|) \times \begin{cases} N(\omega), & \omega > 0 \\ N(|\omega|) + 1, & \omega < 0. \end{cases}$$

Substituting (14a) into (13) gives a homogeneous integral equation for the occupation factor,

$$f(\mathbf{r}; E) = \frac{1}{N_0(\mathbf{r}; E)} \int d\mathbf{r}' \int dE' |G^R(\mathbf{r}, \mathbf{r}'; E)|^2 F(\mathbf{r}', E') \times N_0(\mathbf{r}'; E - E') f(\mathbf{r}'; E - E'). \quad (16)$$

A. Boundary conditions

Two boundary conditions have to be specified, one for G^R in Eq. (12) and one for $f(\mathbf{r}; E)$ in Eq. (16). We take these up one by one.

We use open-ended boundary conditions for $G^R(\mathbf{r}, \mathbf{r}'; E)$ to simulate perfectly absorbing contacts. G^R is calculated numerically using a finite-difference solution to (12) (which is formally equivalent to the tight-binding model) on a finite lattice and extended analytically to $\pm\infty$.³³ This is similar to the asymptotic scattering boundary conditions used by other researchers to calculate a transmission coefficient.³⁴⁻³⁷ However, there is a subtle difference. Usually, the boundary regions are ideal leads with no scattering of any kind extending to ∞ where, presumably, there is an ideal reservoir which is the contact. By contrast, inelastic scattering is included throughout our boundary regions from $-\infty$ to $+\infty$. In our model, the entire boundary region acts as the contact; we do not conceptually divide up the region into an ideal lead and an ideal reservoir.

The integral equation for $f(\mathbf{r}; E)$ is solved subject to the boundary condition that in the contacts

$$f(\mathbf{r}; E) = f_0(E - \mu_i) \quad \text{with } \mathbf{r} \in \text{contact } i$$

where f_0 is the Fermi-Dirac factor. This is similar in

spirit to the boundary condition imposed on the electrostatic potential, and the chemical potentials when solving the drift-diffusion equation.³⁸ Note that we specify the energy distribution rather than the momentum distribution. Usually, it is the incident momentum distribution that is specified as an equilibrium distribution, both in semiclassical³⁹ and quantum transport.^{20,40–43} Despite this difference, in the limit of long τ_ϕ , we find remarkable agreement between simulations based on our approach and simulations from SEQUAL Refs. (34 and 44–46) based on the Tsu-Esaki approach,⁴¹ which assumes phase coherent transport and specifies the incident flux at the boundaries. We also find, for a ballistic wire with M propagating subbands at low temperature and low bias, a conductance of $(2e^2/h)M$. It thus appears that specifying the equilibrium boundary conditions in terms of the energy distribution rather than the incident momentum distribution makes no significant difference to the result. It will be noted that since inelastic scattering is included throughout our boundary regions, energy and momentum are independent variables related through the spectral function. Consequently, it is somewhat more complicated to impose a boundary condition on the momentum distribution.

The concept of an ideal reservoir^{33,42,47–50} has received much attention in the field of electron transport in electron waveguide structures since it is implicit but fundamental to the Landauer conductance formula⁵¹ and multiprobe current formula^{43,52} which have proven so successful in modeling mesoscopic phenomena.⁵³ An ideal reservoir acts as a blackbody for electrons which can be characterized by two properties.

- (i) Every electron incident on the reservoir is absorbed.
- (ii) The reservoir emits electrons according to an equilibrium thermal distribution.

The boundary conditions on G^R and $f(\mathbf{r};E)$ are consistent with the two properties listed above. The open-ended boundary conditions on G^R ensure property (i). Property (ii) is satisfied since we impose equilibrium statistics over the contact region.

The imposition of equilibrium statistics in the contacts gives rise to a contact resistance in the form of a discontinuity in the electrochemical potential at the device-contact interface in the linear-response theory,³³ and, for the nonlinear theory presented here, a discontinuity in $f(z;E)$ at the device-contact interface. If we simulate a ballistic wire, the occupation factor calculated for the wire will be the average of the occupation factors in the contacts $f_w(E) = \frac{1}{2}[f_0(E - \mu_{C_L}) + f_0(E - \mu_{C_R})]$, where $\mu_{C_{L(R)}}$ is the electrochemical potential in the left (right) contact. The contact resistance, which appears as a discontinuity in $f(z;E)$, is a natural result of making the voltage and current measurements between two equilibrium regions.⁴² It must appear if we are to find the two-terminal conductance of $(2e^2/h)M$ for a ballistic wire.

An interesting property of the equilibrium boundary condition is that, while current is conserved in the device, it is not conserved in the contacts. If there is scattering throughout the contact regions, then the contacts must

be in equilibrium far from the device. Thus no current flows deep inside the contacts, although current flows from the contacts into (or out of) the device. The current density decays exponentially away from the device with a decay length $L_\phi = v\tau_\phi$. If scattering is present in the boundary region adjacent to the device, then the same lack of current conservation occurs for the incident equilibrium flux boundary condition used in the Wigner function and Monte Carlo simulations and the Dirichlet boundary conditions used at Ohmic contacts in drift diffusion analysis. For example, in a drift diffusion analysis it is common to assume a constant electrochemical potential μ at the contacts. Thus the current density ($\mathbf{J} = -\sigma \nabla \mu$) is zero inside the contacts although a current flows at the device contact interface. Further discussion of the boundary conditions can be found in Refs. 29 and 33.

In summary, we consider the boundary regions as providing boundary conditions on the “interesting” region, the device. The boundary regions act as ideal reservoirs. We find the correct contact resistance of $2e^2/h$ per mode. We find excellent agreement with the results from SEQUAL, which uses the incident equilibrium flux boundary condition. Current is conserved in the device, but not in the boundary regions. This condition is inherent in equilibrium boundary conditions with inelastic scattering present throughout the boundary region.

B. Current density and current continuity

Equations (12)–(15) are solved iteratively. After convergence, the off-diagonal elements of $G^<$ can be calculated from the general equation $G^< = G^R \Sigma^< G^{R\dagger}$ and then the current density $\mathbf{J}(\mathbf{r};E)$ is calculated from

$$\begin{aligned} \mathbf{J}(\mathbf{r};E) &= \frac{-e\hbar}{4\pi m^*} \lim_{\mathbf{r}' \rightarrow \mathbf{r}} [(\nabla - \nabla') G^<(\mathbf{r}, \mathbf{r}'; E)] \\ &= \frac{-ie\hbar^2}{4\pi m^*} \int \frac{d\mathbf{r}'}{\tau_p(\mathbf{r}'; E)} [G^{R*}(\mathbf{r}, \mathbf{r}'; E) \nabla G^R(\mathbf{r}, \mathbf{r}'; E) \\ &\quad - G^R(\mathbf{r}, \mathbf{r}'; E) \nabla G^{R*}(\mathbf{r}, \mathbf{r}'; E)]. \end{aligned} \quad (17)$$

It is important that the continuity equation

$$\int dE \nabla \cdot \mathbf{J}(\mathbf{r}, E) = 0 \quad (18)$$

be satisfied. Mahan has proven that the continuity equation is satisfied for any self-energy which can be written as $\Sigma^S(\mathbf{x}, \mathbf{x}') = g(\mathbf{x}, \mathbf{x}') G^S(\mathbf{x}, \mathbf{x}')$, where $\mathbf{x} = (\mathbf{r}, t)$ and g is a symmetric function which satisfies $g(\mathbf{x}, \mathbf{x}') = g(\mathbf{x}', \mathbf{x})$.²⁸ This is true of the self-consistent first Born treatment of the electron-phonon interaction. We have, however, ignored the real part of Σ^R in solving the coupled equations (12)–(15). We show below that (18) still holds in our formulation of the coupled equations, (12)–(15).

Starting with Eqs. (17) and (12), we can show that

$$\frac{1}{e} \nabla \cdot \mathbf{J}(\mathbf{r}, E) = \frac{p(\mathbf{r}; E)}{\tau_p(\mathbf{r}; E)} - \frac{n(\mathbf{r}; E)}{\tau_n(\mathbf{r}; E)}. \quad (19)$$

In equilibrium, (19) is a statement of detailed balance and

is equal to zero at each energy.²⁶ This can be seen after noting that, in equilibrium,²⁹

$$\frac{f_0(E)}{\tau_\phi(\mathbf{r};E)} = \frac{1}{\tau_p(\mathbf{r};E)} \quad (20)$$

and

$$\frac{1-f_0(E)}{\tau_\phi(\mathbf{r};E)} = \frac{1}{\tau_n(\mathbf{r};E)}. \quad (21)$$

Away from equilibrium, we must check that the quantity $\int dE \nabla \cdot \mathbf{J}(\mathbf{r};E)$ is zero. We write $1/\tau_n$ and $1/\tau_p$ in (19) using (14), so that (19) integrated over energy becomes

$$\begin{aligned} & \frac{1}{e} \int dE \nabla \cdot \mathbf{J}(\mathbf{r};E) \\ &= \int dE \frac{2\pi}{\hbar} \int dE' [F(\mathbf{r};E-E')n(\mathbf{r};E')p(\mathbf{r};E) \\ & \quad - F(\mathbf{r};E'-E)p(\mathbf{r};E')n(\mathbf{r};E)]. \end{aligned} \quad (22)$$

The right-hand side of (22) is antisymmetric under interchange of E and E' and is thus equal to zero. Thus the divergence of the current in the device is zero. Numerically, we find that the current is conserved throughout the device to within a few percent.

C. Terminal current

The total current flowing at each energy is obtained by integrating $\mathbf{J}(\mathbf{r};E)$ over a cross section of the device. Choosing the cross section to be the device contact interface, we can use the divergence theorem to convert the surface integral into a volume integral over the contact since there is no current flowing out the back of the contact at $\pm\infty$. We can then write the terminal current in an alternate form⁵⁴

$$\begin{aligned} I_1 = \int dE \int_{\mathbf{r} \in C_1} d\mathbf{r} \frac{e\hbar}{2\pi} \int d\mathbf{r}' \frac{|G^R(\mathbf{r},\mathbf{r}';E)|^2}{\tau_\phi(\mathbf{r};E)} \\ \times \left[\frac{f_0(E-\mu_{C_1})}{\tau_\phi(\mathbf{r}';E)} - \frac{1}{\tau_p(\mathbf{r}';E)} \right]. \end{aligned} \quad (23)$$

We have checked numerically that Eq. (23) gives the same result for the terminal current as obtained by integrating the current density over a cross section of the device.

Assuming translational invariance, the 3D quantities in Eqs. (13), (17), and (23) are reduced to 1D quantities by projecting onto the transverse eigenstates and averaging over the cross section. The details are described in Appendix A. Details of the numerical solution of Eqs. (12)–(15) are given in Appendix B.

D. Coherent and incoherent components of the current

The coherent and incoherent contributions to the total current can be calculated from (23) by breaking up the in-

tegral over \mathbf{r}' into two parts as described in Ref. 55. We define the coherent current as that part of total current which traverses the device from one contact to the other without suffering a dephasing event. For a two contact device with contacts C_1 and C_2 sandwiching the “device” with \mathbf{r} in contact C_1 , the integral in (23) would be broken up as follows.

The coherent current is obtained by only integrating \mathbf{r}' in (23) over contact C_2 . Since \mathbf{r}' is constrained to C_2 , we use (20) to write $1/\tau_p(\mathbf{r}';E)$ in (23) as $f_0(E-\mu_{C_2})/\tau_\phi(\mathbf{r}';E)$. Then the coherent current is given by

$$\begin{aligned} I_{\text{coherent}} = \int dE \int_{C_1} d\mathbf{r} \frac{e\hbar}{2\pi} \int_{C_2} d\mathbf{r}' \frac{|G^R(\mathbf{r},\mathbf{r}';E)|^2}{\tau_\phi(\mathbf{r};E)\tau_\phi(\mathbf{r}';E)} \\ \times [f_0(E-\mu_{C_1}) - f_0(E-\mu_{C_2})]. \end{aligned} \quad (24)$$

If we write a transmission coefficient as

$$T(E) = \int_{C_1} d\mathbf{r} \int_{C_2} d\mathbf{r}' \hbar^2 \frac{|G^R(\mathbf{r},\mathbf{r}';E)|^2}{\tau_\phi(\mathbf{r};E)\tau_\phi(\mathbf{r}';E)}, \quad (25)$$

(24) takes the form of the well-known tunneling formula^{40,41}

$$I_{\text{coherent}} = \frac{e}{h} \int dE T(E) [f_0(E-\mu_{C_1}) - f_0(E-\mu_{C_2})]. \quad (26)$$

At first it may seem surprising that the inelastic-scattering times in the contacts enter the expression for the transmission coefficient $T(E)$. We show in Appendix C that the factors of τ_ϕ cancel after performing the integral in (25) and that the transmission coefficient takes the same form as that obtained by Fisher and Lee for coherent transport across the device⁵⁶ (see Appendix C). However, this does not mean that the coherent component of the current is unaffected by inelastic scattering within the device. The quantity $|G^R(\mathbf{r},\mathbf{r}';E)|^2$ in (25) is defined by (12), which includes an imaginary potential proportional to the dephasing rate $i\hbar/2\tau_\phi$. If the dephasing rate is increased in the device, $|G^R|^2$ in (25) is decreased and thus $T(E)$ is decreased.

The incoherent component of the terminal current at C_1 is due to that part of the flux that has suffered a dephasing event in the device. Thus the incoherent component is obtained by restricting the integral over \mathbf{r}' in (23) to the device region. Note that if dephasing is absent in the device, $1/\tau_\phi$ and $1/\tau_p$ in (23) will be zero in the device, and the incoherent component will be zero. As mentioned earlier, the coherent current is obtained by integrating \mathbf{r}' in (23) over C_2 . Also, it can be shown that the contribution from integrating \mathbf{r}' over C_1 gives zero. The sum of the coherent and incoherent components of the current thus add up to the total current as they must.

E. Elastic phase breaking

Elastic phase breaking scattering occurs when the density of oscillator modes $J_0(\hbar\omega)$ is proportional to $\delta(\hbar\omega)$. In this instance, $1/\tau_\phi(\mathbf{r};E) \propto N_0(\mathbf{r};E)$.³³ Since the scattering is elastic, current is conserved at each energy, $\nabla \cdot \mathbf{J}(\mathbf{r};E) = 0, \forall E$.

For purposes of comparison, it is convenient to have the capability of using a constant τ_ϕ independent of position and energy that is not calculated self-consistently so that $1/\tau_\phi$ is not proportional to N_0 . However, we must ensure that current continuity is preserved. Since

$$\frac{1}{e} \nabla \cdot \mathbf{J}(\mathbf{r}; E) = \frac{p(\mathbf{r}; E)}{\tau_p(\mathbf{r}; E)} - \frac{n(\mathbf{r}; E)}{\tau_n(\mathbf{r}; E)},$$

current conservation can be ensured if $n(\mathbf{r}; E)/\tau_n(\mathbf{r}; E) = p(\mathbf{r}; E)/\tau_p(\mathbf{r}; E)$. Dividing both sides by $N_0(\mathbf{r}; E)$ and regrouping gives

$$\frac{1}{\tau_p(\mathbf{r}; E)} = \frac{f(\mathbf{r}; E)}{\tau_\phi(\mathbf{r}; E)}. \quad (27)$$

If we set τ_ϕ constant, then we use (27) to calculate τ_p in place of Eq. (14), and thus ensure current conservation. Examples will be given below of the use of a constant τ_ϕ to simulate dephasing without inelastic transitions.

F. Energy current and power dissipation

The energy current \mathbf{J}_E is

$$\mathbf{J}_E(\mathbf{r}) = \int dE E \mathbf{J}_N(\mathbf{r}; E), \quad (28)$$

where \mathbf{J}_N is the particle current. Note that \mathbf{J}_E is the *total-energy* current, not the kinetic-energy current \mathbf{J}_{E_k} ; $E = E_k + E_c(\mathbf{r})$ where E_k is the kinetic energy and $E_c(\mathbf{r})$ is the potential energy. The power density $P(\mathbf{r})$ due to loss of energy from the electrons to the phonon bath is

$$P(\mathbf{r}) = -\nabla \cdot \mathbf{J}_E(\mathbf{r}). \quad (29)$$

Again, note that in Boltzmann transport theory this is always written as the sum of two terms, a term due to the kinetic energy and a term due to the potential energy,

$$P(\mathbf{r}) = -\nabla \cdot \mathbf{J}_{E_k}(\mathbf{r}) + \mathcal{E}(\mathbf{r}) \cdot \mathbf{J}(\mathbf{r}) \quad (30)$$

[cf. Eq. (7.39) of Ref. 57]. The derivation of (30) from (29) is trivial, but will be shown here since working with total energy is unusual and has caused confusion. Rewrite (28) as

$$\begin{aligned} \mathbf{J}_E(\mathbf{r}) &= \int dE_k \{ [E_c(\mathbf{r}) + E_k] \mathbf{J}_N(\mathbf{r}; E_k) \} \\ &= E_c(\mathbf{r}) \mathbf{J}_N(\mathbf{r}) + \mathbf{J}_{E_k}(\mathbf{r}) \end{aligned}$$

and take the divergence to obtain (30).

G. Mean energy of the current

The mean energy of the current μ_J is defined in 1D as

$$\mu_J = \frac{\int dE E J(z; E)}{\int dE J(z; E)}. \quad (31)$$

For low bias, the heat current is defined in the usual way

as $J_Q = J_E - \mu J_N$, where μ is the electrochemical potential.³⁹ From the definition of μ_J , $J_Q = J_N(\mu_J - \mu)$, and from the definition of the Peltier coefficient (in 1D), $\pi = J_Q/J_N = \mu_J - \mu$. Also, in 1D, the power density is proportional to the slope of μ_J : $P(z) = -dJ_E/dz = -J_N d\mu_J/dz$. For this reason, the concept of μ_J is useful for understanding the location and intensity of power dissipation in devices.

V. RESULTS AND DISCUSSION

The effect of phonon scattering in a simple double-barrier device and in a double-barrier device with an emitter quasibound state will be analyzed. Inelastic scattering will be compared to simple energy broadening such as that obtained from the Breit-Wigner formula. The coherent and incoherent components of the total current will be calculated. By considering the local density of states $N_0(z; E)$, the nonequilibrium occupation of the energy levels $f(z; E)$, the energy spectrum of the current density $J(z; E)$, and the consequent quantities, the mean energy of the current density μ_J and the power density $P(z)$ throughout the device, we will obtain a clear picture of the effect of the electron-phonon scattering on the electron transport.

A. Device description

The first device that is modeled is a simple double barrier resonant-tunneling diode. The conduction band for the device is shown in Fig. 1. The temperature is 77 K. A constant effective mass of 0.067 is used. The barrier-well conduction-band discontinuity is 220 meV. A linear potential drop is applied. The electrostatic potential is not calculated self-consistently. The lattice constant for the spatial grid is 5 Å.

B. Comparison with coherent transport

Fig. 2 shows a comparison of I - V characteristics. The dashed line is the output of the program SEQUAL,^{34,44-46}

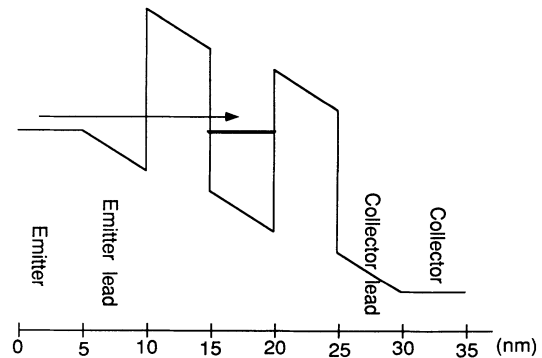


FIG. 1. Conduction-band profile of simple double-barrier resonant-tunneling diode considered in Figs. 2–8. $T = 77$ K, $m^* = 0.067m_0$, $\Delta E_c = 220$ meV, $a = 5$ Å.

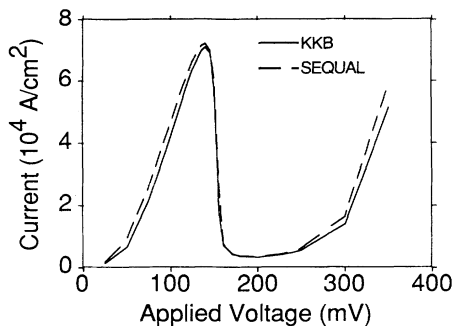


FIG. 2. Comparison of the results of simulator based on the Keldysh formalism (KKB) with the results of SEQUAL which assumes phase-coherent transport. A constant τ_ϕ of 10 ps is used in the KKB simulator.

which is based on Eq. (26) and assumes phase-coherent transport from contact to contact. Furthermore, the boundary conditions in SEQUAL are specified by an equilibrium incident momentum distribution. The solid line is the output from our quantum kinetic equation solver, labeled KKB, with the phase relaxation time set equal to a constant value, independent of position and energy, of 10 ps. The imaginary term in Eq. (12) is 0.033 meV. This is a factor of 20 smaller than the smallest energy scale in the problem, which is the resonance width. Thus we are approximating a pure-state retarded Green's function $G^R = (E - H_0 + i\delta)^{-1}$, by letting the infinitesimal imaginary term $i\delta$ become nonzero but small. In this limit, the current is essentially given by (24), which is identical to (26). Thus, in this limit, we would expect the two simulators to give the same result. Figure 2 shows that this is indeed the case.

The two simulators not only differ in their theoretical basis, but they also differ in their numerical approach. SEQUAL solves for the transmission coefficient $T(E)$ using a scattering matrix approach. The potential is discretized into a series of steps and the plane-wave eigenstates of each step are matched at the step boundaries. Thus the dispersion relation is parabolic for all energies above the conduction band. The KKB solver uses finite difference to solve (12), which is equivalent to tight binding,³³ so that the dispersion relation is $E = (\hbar^2/ma^2)[1 - \cos(ka)]$. The inflection point of the tight-binding band, using the lattice constant and effective mass stated above, occurs at $E = 4.5$ eV. At high applied voltages, when the electrons come through the resonance high into the tight-binding band of the collector, one would expect a difference in the predictions of the two simulators.

C. Elastic phase breaking versus inelastic scattering

In Fig. 3, the effect of inelastic scattering is compared to elastic energy broadening. For the solid line, both Debye and Einstein oscillators are present. The strengths of the two scattering mechanisms are chosen such that at $5k_B T + \hbar\omega_0$ above the Fermi energy in the emitter, the scattering rate, associated with the retarded self-energy

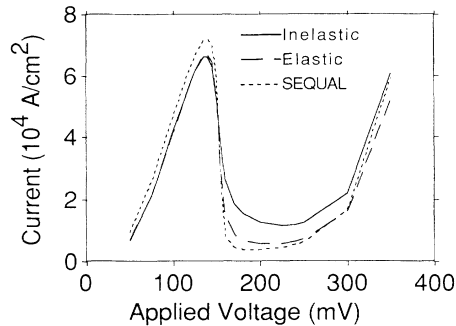


FIG. 3. Comparison of inelastic scattering, elastic phase-breaking scattering, and phase-coherent transport (SEQUAL). For the solid curve, both Debye and Einstein oscillators are present. For the long-dashed curve, only elastic phase breaking is present; in the well, $\tau_\phi = 0.46$ ps.

$1/\tau_0$ due to optical phonons is $\sim 10^{13} \text{ s}^{-1}$ and the scattering rate due to the Debye oscillators is $\sim 10^{12} \text{ s}^{-1}$. At nondegenerate energies, the rate $1/\tau_\phi$ should be similar to that calculated from Fermi's golden rule. The rate $1/\tau_\phi$ is calculated self-consistently with $G^<$ and, therefore, is position and energy dependent and decreases with decreasing energy.

At peak current, between the barriers, τ_ϕ varies with energy from 0.53 ps at the bottom of the resonance to 0.07 ps one optical phonon energy above the bottom of the resonance.⁵⁸ To compare with elastic phase breaking, using a constant τ_ϕ , we have calculated an average τ_ϕ using the energy distribution of the current density as a weighting factor. That is

$$\langle \tau_\phi(z_0) \rangle = \frac{\int dE \tau_\phi(z_0; E) J(z_0; E)}{\int dE J(z_0; E)},$$

where z_0 is the point in the center of the well. The value for $\langle \tau_\phi(z_0) \rangle$ is 0.46 ps. At the node in the emitter contact at the contact-device interface $\langle \tau_\phi \rangle = 0.8$ ps.

For the long-dashed line in Fig. 2, τ_ϕ is set to a constant 0.46 ps in the resonance region and 0.8 ps in the contacts. As described previously, this results in elastic phase breaking. Thus the energy broadening is roughly the same for the two different simulations; however, in one case there is inelastic scattering present; in the other case, there is not. Also, replotted from Fig. 2 is the result from SEQUAL (dotted line).

Comparing the inelastic and elastic I - V characteristics, the shape of the linear and peak part of the I - V curves is the same for both cases. The difference between the two curves lies in the magnitude of the valley current. When there is inelastic scattering present, the valley current is slightly larger because electrons can enter the well at high energy and inelastically scatter down into the resonance thus enhancing the current. For both curves, the peak current is slightly less than and the valley current is more than the result from SEQUAL.

D. Coherent versus sequential tunneling

Since Luryi first introduced the alternative explanation of the I - V characteristic of a DBRTD based on the sequential tunneling picture,⁵⁹ there has been interest in determining the fraction of the total current that is coherent and incoherent.^{7,60} For the I - V curve of Fig. 3 with inelastic scattering present, we have plotted the coherent and incoherent components [Fig. 4(a)]. Initially, before the peak current is reached, the coherent part is the larger. For the valley current, the incoherent component is larger. This is due to electrons scattering down from their injected energy into the resonance. Past the valley current, the coherent component again becomes larger.

We compare this to Fig. 4(b) in which the elastic curve of Fig. 3 is replotted along with its coherent and incoherent components. For this simulation, τ_ϕ is kept fixed as described above so that it does not vary with voltage. The current is evenly split between its coherent and incoherent components.

A Breit-Wigner analysis indicates that the ratios of the coherent and incoherent components of the current are inversely related to the intrinsic time and the phase-breaking scattering time $I_{\text{coherent}}/I_{\text{incoherent}} = \tau_\phi/\tau_{\text{intrinsic}}$.⁶ We estimate the intrinsic time using the relation $\hbar/\tau_{\text{intrinsic}} = \Delta E$, where ΔE is the full width at half maximum of $N_0(z_0; E) = (-1/\pi)\text{Im}G^R(z_0, z_0; E)$ at the well center at a bias of 135 mV (peak current) with $\tau_\phi = 10$ ps.

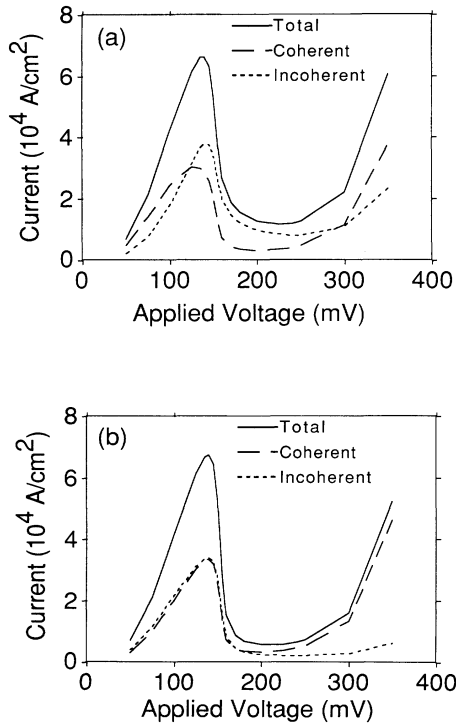


FIG. 4. Coherent and incoherent components of the total current. The (a) solid and (b) dashed curves of Fig. 3 are replotted. The coherent (long dash) and incoherent (dot) components are shown.

At peak current, for Fig. 5(b), $I_{\text{coherent}}/I_{\text{incoherent}} = 0.99$ and $\langle \tau_\phi \rangle / \tau_{\text{intrinsic}} = 1.0$. Thus, if we use a constant time for τ_ϕ , we find good agreement with the prediction of a Breit-Wigner analysis.

E. Scattering rates: Energy and bias dependence

The energy and bias dependence of τ_ϕ , and the inter-relationship between the nonequilibrium occupation factor f , the 3D density of states N_0 , and the inelastic-scattering time τ_ϕ in the self-consistent first Born approximation are demonstrated in Figs. 5(a) and 5(b). Figures 5(a) and 5(b) are overlays of cross sections taken in position at the well center for the above three quantities plotted versus *total* energy occurring at the peak current and valley current, respectively, of Fig. 3. The quantities correspond to the simulation with inelastic scattering present. The scale for τ_ϕ is on the left axis. The scale for N_0 is the right axis. The scale for f is not shown, but runs linearly from 0 to 1. Note that N_0 is the 3D density of states which contains all transverse energies. We now discuss the inter-relationships between the three quantities.

The feature in τ_ϕ at point B in Figs. 5(a) and 5(b) is due to the turn on of optical-phonon emission. Point B lies one optical-phonon energy above the resonance bottom.

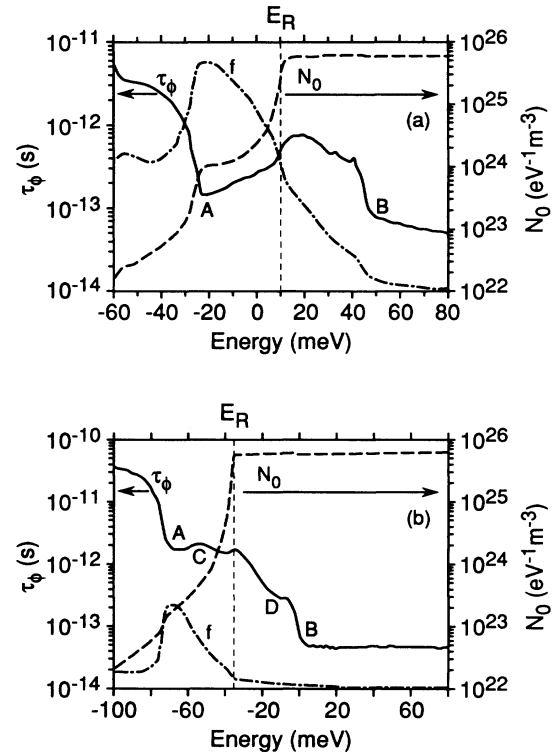


FIG. 5. Overlay of $f(z_0; E)$, $N_0(z_0; E)$, and $\tau_\phi(z_0; E)$ at (a) peak current 135 mV and (b) valley current 225 mV. z_0 is the fixed point in the center of the well. The scale for f is not shown, but runs linearly from 0 to 1. E_r is the energy of the bottom of the resonance.

In Fig. 5(a), there is a corresponding feature in f which will be studied more closely in Fig. 6. At point A , one optical-phonon energy below the resonance, there are prominent features in all of the quantities. There is a peak and precipitous dropoff in the occupation factor f . This is the result of electrons scattering down from the resonance to fill the exponentially vanishing states below the resonance. A bump in the density of states also occurs, and there is a sharp decrease in τ_ϕ . In the KKB theory, this decrease in τ_ϕ is formally associated with the emission of phonons by holes (in the conduction band). The small features at points C and D in τ_ϕ correspond to one Debye cutoff energy, 20 meV, below and above the resonance.

in Fig. 5(b), the conduction band in the emitter is above the level of the resonance and the resonance is $24k_B T$ above the Fermi energy of the collector. Thus the small occupation of the resonance level ~ 0.03 is due to inelastically scattered electrons from the emitter. Since the occupation is negligible, Fermi's golden rule should be a good approximation to the scattering time τ_ϕ . This is correct above the resonance. Below the resonance, the scattering time is dominated by the hole scattering rate, $1/\tau_p$ as discussed below.

The sudden increase in $1/\tau_\phi$ at point A is not due to absorption of optical phonons by electrons. $1/\tau_\phi$ is the imaginary part of Σ^R and it is the sum of the electron out-scattering rate $1/\tau_n$ and the hole outscattering rate $1/\tau_p$. This results from the proper treatment of the Pauli exclusion principle built into the KKB formalism.²² For dispersionless optical phonons, the calculation of $1/\tau_p$ and $1/\tau_n$ is particularly simple:

$$\frac{1}{\tau_n(E)} \propto N(\omega_0)N_0(E + \hbar\omega_0)[1 - f(E + \hbar\omega_0)] + [N(\omega_0) + 1]N_0(E - \hbar\omega_0)[1 - f(E - \hbar\omega_0)], \quad (32a)$$

$$\frac{1}{\tau_p(E)} \propto N(\omega_0)N_0(E - \hbar\omega_0)f(E - \hbar\omega_0) + [N(\omega_0) + 1]N_0(E + \hbar\omega_0)f(E + \hbar\omega_0). \quad (32b)$$

N is the Bose-Einstein factor, N_0 is the electron density of states, f is the electron occupation factor, and $\hbar\omega_0$ is the optical-phonon energy. The position coordinate \mathbf{r} has been suppressed. In (32), letting E be the energy of point A , one finds that the second term of (32b) is the largest. This represents the emission of optical phonons by holes, which is identical to the emission of optical phonons by electrons one optical-phonon energy above point A . At point B , the second term in (32a) dominates, which represents the emission of optical phonons by electrons.

The slight increase in τ_ϕ after point A is due to the decrease in $f(E)$ above the resonance. Point C occurs one Debye cutoff energy below the resonance. The Debye oscillators cannot start contributing to the rate $1/\tau_\phi$ until the energy is within a Debye cutoff of the resonance. The increase in $1/\tau_\phi$ between the points A and B is due to the Debye oscillators. At energies higher than the resonant

energy, the scattering due to the Debye oscillators is dominated by emission by electrons. Above point B , τ_ϕ is determined by the second term in (32a). $N_0(E - \hbar\omega_0)$ is constant, $f(E - \hbar\omega_0)$ is negligible; thus τ_ϕ becomes a constant. Contrasting with point B in Fig. 5(a), τ_ϕ is not constant, but decreasing since $f(E - \hbar\omega_0)$ is not negligible.

Thus, at energies above resonance, when $f(E - \hbar\omega_0)$ can be ignored, τ_ϕ is given by the same terms as found in Fermi's golden rule. However, there is a difference. Fermi's golden rule treats the one-phonon interaction to first order, while the SCFBA treats the one-phonon interaction to all orders. Thus, in the SCFBA, the density of states is affected by the scattering rate. This effect is seen at point A in Fig. 5(a) and point B in Figs. 5(a) and 5(b) [there is a slight decrease in $N_0(E)$ with increasing energy].

To summarize the above discussion of Fig. 5, below the resonance, τ_ϕ is determined by a term in the KKB formalism that corresponds to the emission of phonons by holes. This term would be absent in a one-electron picture. It affects the shape of the tail of the resonance. Above the resonance bottom, τ_ϕ is dominated by emission of phonons by electrons, and the terms in the expression are the same terms that appear in Fermi's golden rule when the occupation factor can be ignored. The feedback between τ_ϕ and N_0 in the SCFBA alters the density of states.

F. Nonequilibrium distribution function

Inelastic scattering affects the equilibration of energy levels in the resonance. We demonstrate this in Fig. 6. In Fig. 6, we plot the occupation factor in the center of the well at peak current for the inelastic and elastic I - V curves of Fig. 3, the KKB curve from Fig. 2, now labeled "Coherent," and the tail of a Fermi-Dirac function with a Fermi energy 4 meV below the resonance and a temperature of 205 K

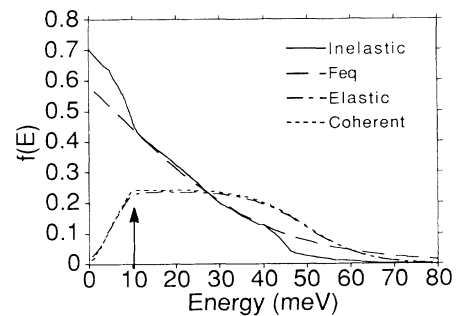


FIG. 6. $f(E)$ at the well center at peak current (135 mV) for the three cases of inelastic scattering, elastic phase-breaking scattering (from Fig. 3), and coherent transport (from solid curve, Fig. 2). The tail of a Fermi-Dirac function with a Fermi energy 4 meV below the resonance and a temperature of 205 K is also plotted (Feq). The arrow lies at the energy of the bottom of the resonance, 10 meV.

ature of 205 K labeled "Fq." The arrow represents the energy of the bottom of the resonance.

When only elastic phase breaking is present, the sequential tunneling picture predicts that the occupation of the well should be proportional to the occupation in the emitter.⁶¹ This is what we find. Above the bottom of the resonance, the occupation in the well for both the elastic and coherent curve is a scaled version of the equilibrium Fermi-Dirac factor in the emitter. For the elastic curve, τ_ϕ is set to a constant value in the well of 0.46 ps and for the coherent curve, τ_ϕ is set to 10 ps. There is essentially no difference in the occupation of the well for the two cases. With only elastic phase-breaking processes, the different energies are in disequilibrium, and the occupation factor cannot be fit to the tail of a Fermi-Dirac function.

When inelastic scattering is present (solid line), the electron-state occupation is shifted to lower energies as expected. Furthermore, the occupation above the resonance can be fit fairly well to the tail of a Fermi-Dirac function (long-dashed line). The fit is good for energies above the resonance and below the threshold for optical-phonon emission $E_r < E < E_r + \hbar\omega_0$. At energies above the optical-phonon energy, there is a depletion in the calculated occupation factor compared to the equilibrium factor. This is precisely what is expected. As pointed out by Yang *et al.*³⁶ and Hess,⁶³ rapid optical-phonon scattering tends to deplete the distribution of carriers with kinetic energies larger than the phonon energy. The phonons tend to cut off the high-energy part of the Boltzmann tail. This is what is shown by our simulations.

G. Energy distribution of the current

The energy distribution of the current density gives us information about the inelastic scattering and power dissipation within the device. In the following plots, Figs. 7 and 8, we consider the spatial variation of the inelastic-scattering intensity and power dissipation. We find a relatively high intensity of inelastic scattering and power dissipation in the resonant regions.

The energy distribution of the current density $J(z;E)$ at the bottom of the valley current (225 mV in Fig. 3) with inelastic scattering present is plotted versus position and energy in Fig. 7(a). The current enters at the high energy of the emitter, the right side, and the energy distribution changes very little until the 5-nm region of the well. Then there is a major shift in the distribution from the high incoming energy down to the bottom of the resonance level where the distribution peaks sharply. This is shown clearly in Fig. 7(b) where two cross sections taken from Fig. 7(a) along lines of constant position are plotted. Both curves are taken from a point 1 nm outside the well in the adjacent barrier. The long-dashed curve is from the emitter barrier, and the solid curve is from the collector barrier. The points on the energy axis labeled E_R , E_C , and E_F are the energies of the resonance, the emitter conduction band, and the emitter Fermi level, respectively. Exiting the well, there is little change in the distribution in the collector barrier and lead. Thus the well is a

region of relatively intense inelastic scattering compared to the leads.

This result seems reasonable on physical grounds. In the resonance, the group velocity of the electrons is slow compared to the surrounding regions. If the inelastic-scattering time is roughly position independent, then the inelastic-scattering length is shorter in the resonance region than in the leads and a higher intensity of energy relaxation results. Defining the power density as the power dissipated by the electrons to the phonon bath, then a peak in the power density results in the region of the resonance.

H. Power density

The mean energy of the current density μ_J is plotted versus position in Fig. 8(a) for the peak current, 135 mV, and the valley current, 225 mV, of Fig. 3 when inelastic scattering is present. This shows clearly the relatively large drop in energy that occurs in the well. μ_J is defined such that the power density is proportional to its derivative $P(z) = -J_N(d/dz)\mu_J$. The power density, plotted in Fig. 8(b), shows a large peak in the 5-nm region of the well.

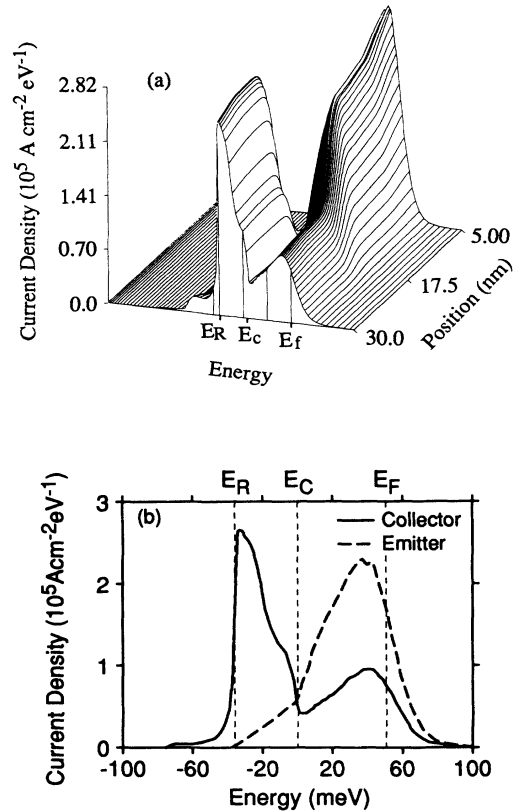


FIG. 7. (a) $J(z;E)$ plotted vs position and energy at 225 mV with inelastic scattering. E_f is the Fermi energy of the emitter, E_c is the level of the conduction band in the emitter, and E_r is the energy of the bottom of the resonance. (b) Cross sections from (a) at constant position 1 nm outside the well in the emitter and collector barrier.

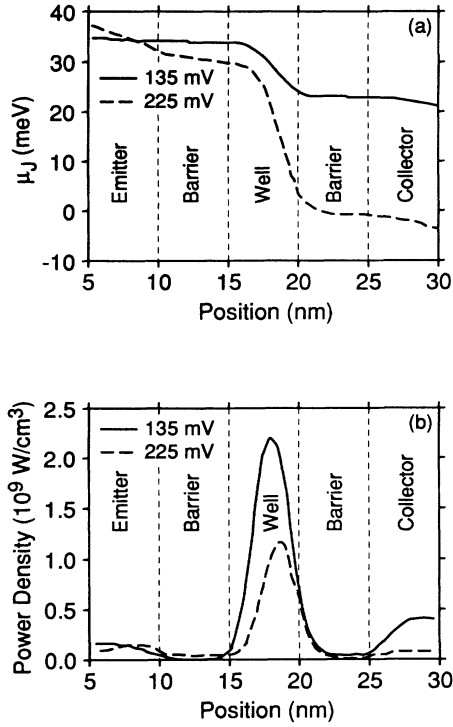


FIG. 8. (a) Mean energy of the current density $\mu_J(z)$ at 135 and 225 mV. (b) Power density $P(z)$ at 135 and 225 mV.

Although most of the power loss seems to be occurring in the well, most of the $I \times V$ loss is actually occurring in the contacts (not shown) as in the usual Landauer picture.⁶⁴ Only the device region has been plotted in Figs. 8(a) and 8(b). The total integrated power $\int dz P(z)$ in Fig. 8(b) (225 mV) is $\sim 0.18 I \times V$. In a real device, the leads are metallic n^+ material and they are very long, micrometers instead of nanometers. Very deep in the emitter and collector leads the current is distributed in energy as it would be in an n^+ resistor. The mean energy of the current μ_J would lie a distance π (the Peltier coefficient) above the quasi-Fermi energy μ . Since the applied bias is 225 mV, μ_J must drop by 225 meV across the real device. In Fig. 8(a), the total drop across the “device” is ~ 41 meV, which gives the factor of 0.18. Thus, in a real device, the majority of the power dissipation is taking place in the leads and contacts. There is simply a peak in the power density in the resonance region.

The concept of the mean energy of the current density μ_J provides a way of qualitatively understanding the location and intensity of the power dissipation in devices and placing upper limits on the amount of power dissipated in any one region. In 1D, when $\mathbf{J} = J\hat{z}$, $P(z) = -dJ_E(z)/dz = -J_N d\mu_J/dz$. The net power being dissipated between points z_0 and z_1 is $J_N[\mu_J(z_0) - \mu_J(z_1)]$, where J_N is the particle current. Thus the net power dissipated in a region is proportional to the drop in μ_J in that region.

As an example, consider the peak current of the device (135 mV). In the Luryi picture,⁵⁹ at zero temperature, μ_J in the emitter lead equals $E_F/2$ where E_F is the Fermi

energy of the emitter contact, and the energy of the bottom of the emitter conduction band is taken to be zero. Since the bottom of the emitter conduction band is aligned with the bottom of the resonance in the well, the maximum drop possible in μ_J between the barriers is $E_F/2$. Thus the maximum power that can be dissipated between the barriers is $J_N E_F/2$, where J_N is the particle current density. For Fig. 8, this estimate is a factor of 5 higher than the calculated power dissipated in the well.

I. Effect of a quasibound state in the emitter

Next, the effect of inelastic scattering in a resonant tunneling device with an emitter quasibound state is considered. The conduction band, superposed over a gray scale plot of the calculated, strictly 1D density of states, $N_0(z; E)$ is shown in Fig. 9. The temperature, effective mass, and conduction-band offsets are the same as described for Fig. 1. A linear potential drop is used, and the I - V characteristic is shown in Fig. 10. The contribution to N_0 from the transverse energies has been ignored in the plots for clarity. The dark regions present high density of states. The resonance level and quasibound states in the triangular well of the emitter lead can be seen. There is also a standing-wave pattern due to reflection from the barriers on either side of the barriers.

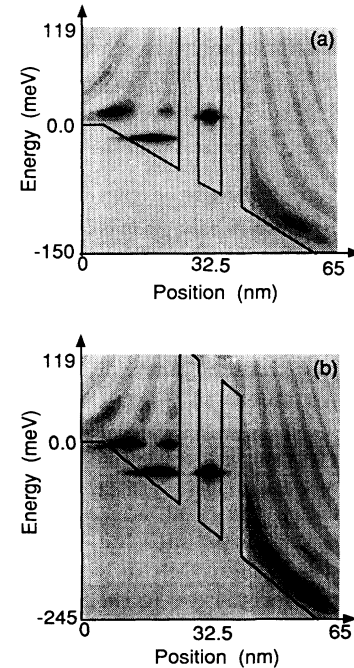


FIG. 9. Shadow plots of the calculated, strictly 1D density of states $N_0(z; E)$, with conduction-band profile superposed corresponding to (a) the first current peak, 150 mV, and (b) the second current peak, 245 mV of Fig. 10. Dark regions are regions of high density of states. The contribution of states from the transverse energies have been ignored in the plot for clarity.

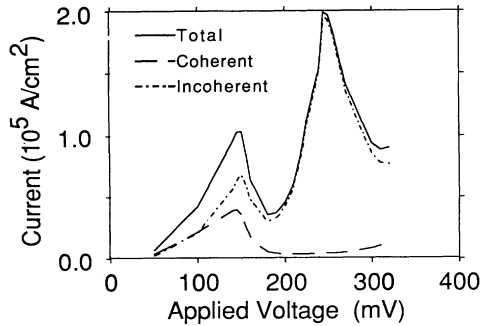


FIG. 10. I - V characteristic for DBRTD of Fig. 9. The total current is plotted along with its coherent and incoherent components.

The first peak in the I - V characteristic corresponds to the conduction band in the emitter crossing the resonance level in the well [Fig. 9(a)]. The second peak occurs when the quasibound state in the emitter lead aligns with the resonance in the well [Fig. 9(b)]. Also plotted in Fig. 10 are the coherent and incoherent parts of the current. The coherent current is the fraction of the total current that has crossed the entire device, from the emitter at 5 nm to the collector at 60 nm, coherently. In Fig. 9(b), all of the current flowing is incoherent. All of the current is coming from the emitter, inelastically scattering down into the quasibound state and flowing

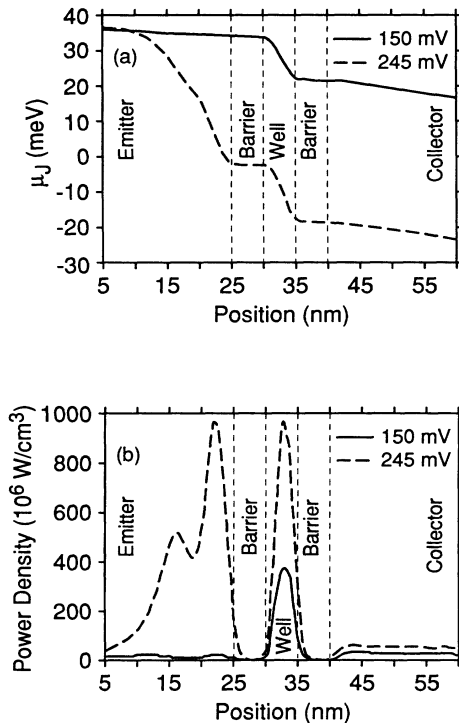


FIG. 11. (a) Mean current energy $\mu_J(z)$ corresponding to the two current peaks of Fig. 10. (b) Power density $P(z)$ corresponding to the two current peaks.

out through the resonance. At the first current peak [Fig. 9(a)], no current is flowing through the quasibound state. This is clearly shown in plots of the mean current energy.

The mean current energy μ_J is plotted in Fig. 11(a). For the first current peak, the slope of μ_J is smallest in the emitter lead, next largest in the collector lead, and largest in the well. This ordering is expected since the power density is proportional to $d\mu_J/dz$. The maximum power density is in the resonance region. In the collector region, where there is plenty of phase space into which to scatter, the power density is greater than in the emitter lead. The lack of drop in the emitter lead indicates that no current is flowing through the emitter quasibound state. At the second current peak, 245 mV, there is a large drop in μ_J in the emitter lead. This is what must occur if current is to flow through the emitter quasibound state.

The power density for the two current peaks is shown in Fig. 11(b). At 150 mV, there is a peak in the power density in the well only. At 245 mV, there are large peaks both in the well and in the emitter lead corresponding to the two quasibound states. Again, the same cautionary word is in order. Figure 11(b) does not imply that the majority of the I - V power loss is occurring in the quasibound states. The drop in μ_J in the emitter lead at a bias of 245 mV is 39 meV. Thus $\frac{39}{245}$ (0.16) of the I - V power is being dissipated in the emitter quasibound state; $\frac{16}{245}$ (0.065) of the I - V power is dissipated between the barriers, the majority of the power is still being dissipated in the contacts.

VI. SUMMARY AND CONCLUSION

The nonequilibrium Green's-function approach provides a powerful tool for investigating the effect of energy broadening and inelastic scattering in quantum transport. The effects of both constant and energy dependent self-energies calculated in the self-consistent first Born approximation can be compared. Our approach allows the energy spectrum of the phonons to be included, and it allows a self-consistent first Born treatment of the electron-phonon interaction. It also allows the calculation of a number of quantities which give insight into the effect of inelastic processes on quantum electron transport throughout the device. The nonequilibrium occupation factor $f(z;E)$ shows the effect of inelastic scattering on the equilibration of energy levels. With inelastic scattering present, the occupation of the well of the simple resonant tunneling structure at the peak current can be described by the tail of a Fermi-Dirac factor up to the optical-phonon energy at which point the calculated f is depleted. With no inelastic scattering, the occupation of the well is a scaled version of the occupation in the emitter. The local density of states $N_0(z;E)$ displays how different resonances align with each other and with the conduction band. We have shown that the enhanced valley current due to inelastic scattering is coincident with enhanced occupation of the resonant state. The process of filling the state also is seen in the energy-dependent current density $J(z;E)$, which undergoes a sharp down-

ward shift in the resonance region. This shows up as a peak in the power density between the barriers. Knowing $J(z;E)$, one can calculate the mean current energy μ_J and hence the power density throughout the device.

The concept of the mean current energy was introduced and shown to be a valuable intuitive tool by which to understand the spatial variation and intensity of the power dissipation. The mean energy of the current density indicates where power is being dissipated in a device. We have consistently found peaks in the power density when current passes through a resonance; however, only a fraction of the total I - V power is actually dissipated there.

Thus, by including the energy coordinate explicitly and performing energy-resolved computations, one can calculate the occupation of levels $f(z;E)$, the local density of states $N_0(z;E)$, the energy distribution of the current density $J(z;E)$, the mean energy of the current μ_J , and the power density throughout the device. These quantities provide a detailed picture of the effect of inelastic transitions on quantum transport.

Note added in proof. We note several theoretical studies of the effect of inelastic scattering in double-barrier resonant tunneling that were missed in the Introduction,^{65–68} and several works that have recently appeared.^{69–72} Special mention needs to be made of the work of Anda and Flores,⁶⁹ whose model and treatment are very close to ours. Both approaches are based on the Keldysh formalism, though the detailed implementation is different. Also, they treat strictly 1D resonant-tunneling diodes while we treat 1D resonant-tunneling diodes with finite cross section.

ACKNOWLEDGMENTS

The software used to produce the numerical results is a modified and extended version of a program originally written by Michael McLennan who has also provided guidance for the use of SEQUAL. One of us (R.L.) ac-

knowledges a helpful discussion with William Frensley and discussions with Mark Stettler and Muhammad Alam. This work was supported by the Semiconductor Research Corporation under Contract No. 90-SJ-089.

APPENDIX A: INFINITE CROSS SECTION

To simulate a device with translational invariance, we wish to only compute one dimensional quantities. We achieve this by averaging Eqs. (13), (17), and (23) over the transverse plane. The derivation that follows is identical in spirit to a simpler derivation by McLennan in which only the case of a constant τ_ϕ , independent of position and energy, was considered.⁷³ We assume a separable Hamiltonian. Furthermore, since the system is translationally invariant, we assume that the occupation factor $f(\mathbf{r};E)$ and the phase relaxation time $\tau_\phi(\mathbf{r};E)$ are not functions of the transverse coordinates. Thus the transverse eigenfunctions of the Hamiltonian

$$H_\tau(\mathbf{r};E) = H_0(\mathbf{r}) - i\hbar/\tau_\phi(\mathbf{r};E) \quad (\text{A1})$$

are plane waves.

We will take Eq. (13) as an example. The transverse coordinates are x and y , and the longitudinal coordinate is z . We begin by multiplying both sides of (13) by $N_0(\mathbf{r};E)$ and then averaging both sides over the cross section. Considering the left-hand side first, we have

$$f(z;E) \frac{1}{W_x W_y} \int dx dy N_0(x,y,z;E). \quad (\text{A2})$$

Next, we write N_0 as $-\text{Im}G^R(\mathbf{r},\mathbf{r};E)/\pi$ and expand G^R in terms of the eigenfunctions of (A1). Since we have assumed that τ_ϕ is only a function of z , the transverse part of H_τ is Hermitian with plane-wave eigenfunctions. The z component is non-Hermitian and is expanded in terms of the eigenfunctions $\chi_n(z)$ and $\eta_n(z)$ of the adjoint operators $H_\tau(z)$ and $H_\tau^*(z)$.⁷⁴ Equation (A2) becomes

$$f(z;E) \frac{1}{W_x W_y} \int dx dy \frac{-1}{\pi} \text{Im} \sum_{l,m,n} \frac{\phi_l(x)\phi_m(y)\chi_n(z)\phi_l^*(x)\phi_m^*(y)\eta_n^*(z)}{E - \epsilon_l - \epsilon_m - \epsilon_n}. \quad (\text{A3})$$

ϕ_l and ϕ_m are plane wave eigenstates, $\phi_l(x) = \exp(ik_l x)/\sqrt{W_x}$. ϵ_l and ϵ_m are the corresponding eigenenergies. ϵ_n is the complex eigenvalue corresponding to χ_n and η_n^* . Since the plane waves appear with their complex conjugates, they disappear from (A3), and (A3) becomes

$$f(z;E) \frac{1}{W_x W_y} \frac{-1}{\pi} \text{Im} \sum_{l,m,n} \frac{\chi_n(z)\eta_n^*(z)}{E - \epsilon_l - \epsilon_m - \epsilon_n}. \quad (\text{A4})$$

We rewrite the term $(-1/\pi)\text{Im}\sum_{l,m,n}$ in (A4) as

$$\sum_{l,m} N_0^{\text{1D}}(z;E - \epsilon_l - \epsilon_m), \quad (\text{A5})$$

where N_0^{1D} is the density of states obtained from only considering the z component of H_τ . Defining a quantity $\langle N_0 \rangle$ as

$$\begin{aligned} \langle N_0(z;E) \rangle &= \frac{1}{W_x W_y} \sum_{l,m} N_0^{\text{1D}}(z;E - \epsilon_l - \epsilon_m) \\ &= \frac{m^*}{2\pi\hbar^2} \int_{-\infty}^E dE' N_0^{\text{1D}}(z;E'), \end{aligned} \quad (\text{A6})$$

(A4) becomes

$$f(z;E) \langle N_0(z;E) \rangle. \quad (\text{A7})$$

Now we consider the right-hand side of (13). We sub-

stitute (14a) into (13) and average over the cross section to obtain

$$\frac{1}{W_x W_y} \frac{\hbar}{2\pi} \int dE' \int dz' \int dx dy dx' dy' \times [|G^R(\mathbf{r}, \mathbf{r}'; E)|^2 N_0(\mathbf{r}'; E') f(z'; E') F(E - E')] . \quad (\text{A8})$$

The integral

$$\frac{1}{W_x W_y} \int dx dy dx' dy' |G^R(\mathbf{r}, \mathbf{r}'; E)|^2 N_0(\mathbf{r}'; E') \quad (\text{A9})$$

is evaluated by expanding $|G^R|^2$ and N_0 in terms of the eigenfunctions of H_r . Writing out the expansion, (A9) becomes

$$\frac{1}{W_x W_y} \int dx dy dx' dy' \left[\sum_{l,m,n} \frac{\phi_l(x) \phi_m(y) \chi_n(z) \phi_l^*(x') \phi_m^*(y') \eta_n^*(z')}{E - \varepsilon_l - \varepsilon_m - \varepsilon_n} \times \sum_{l',m',n'} \frac{\phi_{l'}^*(x) \phi_{m'}^*(y) \chi_{n'}^*(z) \phi_{l'}(x') \phi_{m'}(y') \eta_{n'}(z')}{E - \varepsilon_{l'} - \varepsilon_{m'} - \varepsilon_{n'}} \times \frac{-1}{\pi} \text{Im} \sum_{i,j,k} \frac{\phi_i(x') \phi_j(y') \chi_k(z') \phi_i^*(x') \phi_j^*(y') \eta_k^*(z')}{E - \varepsilon_i - \varepsilon_j - \varepsilon_k} \right] . \quad (\text{A10})$$

The third term in the integrand of (A10) is $\langle N_0(z; E) \rangle$. The integrals over x' and y' give factors of $\delta_{l,l'}$ and $\delta_{m,m'}$, respectively. $1/W_x W_y$ times the integral of the first two terms in the integrand of (A10) becomes

$$\frac{1}{W_x W_y} \sum_{l,m} \left[\sum_n \frac{\chi_n(z) \eta_n^*(z')}{E - \varepsilon_l - \varepsilon_m - \varepsilon_n} \sum_{n'} \frac{\chi_{n'}^*(z) \eta_{n'}(z')}{E - \varepsilon_l - \varepsilon_m - \varepsilon_{n'}} \right] . \quad (\text{A11})$$

The quantity in (A11) is

$$\frac{1}{W_x W_y} \sum_{l,m} |G_{\text{ID}}^R(z, z'; E - \varepsilon_l - \varepsilon_m)|^2 , \quad (\text{A12})$$

where G_{ID}^R is the retarded Green's function of the z component of H_r . We define the quantity $\langle |G^R|^2 \rangle$ as

$$\begin{aligned} \langle |G^R(z, z'; E)|^2 \rangle &= \frac{1}{W_x W_y} \sum_{l,m} |G_{\text{ID}}^R(z, z'; E - \varepsilon_l - \varepsilon_m)|^2 \\ &= \frac{m^*}{2\pi \hbar^2} \int_{-\infty}^E dE' |G_{\text{ID}}^R(z, z'; E')|^2 . \end{aligned} \quad (\text{A13})$$

Putting this all back together, Eq. (13) becomes

$$f(z; E) = \frac{\hbar}{2\pi} \frac{1}{\langle N_0(z; E) \rangle} \int dz' \frac{\langle |G^R(z, z'; E)|^2 \rangle}{\langle \tau_p(z'; E) \rangle} , \quad (\text{A14})$$

where

$$\left[E' + \frac{\hbar^2}{2m^*} \frac{d^2}{dz^2} - V(z) + \frac{i\hbar}{2\langle \tau_p(z; E) \rangle} \right] G_{\text{ID}}^R(z, z'; E') = \delta(z - z') , \quad (\text{A15})$$

$$\frac{1}{\langle \tau_p(z; E) \rangle} = \frac{2\pi}{\hbar} \int dE' F(E - E') \langle N_0(z; E') \rangle f(z; E') , \quad (\text{A16})$$

$$\frac{1}{\langle \tau_n(z; E) \rangle} = \frac{2\pi}{\hbar} \int dE' F(E' - E) \langle N_0(z; E') \rangle \times [1 - f(z; E')] \quad (\text{A17})$$

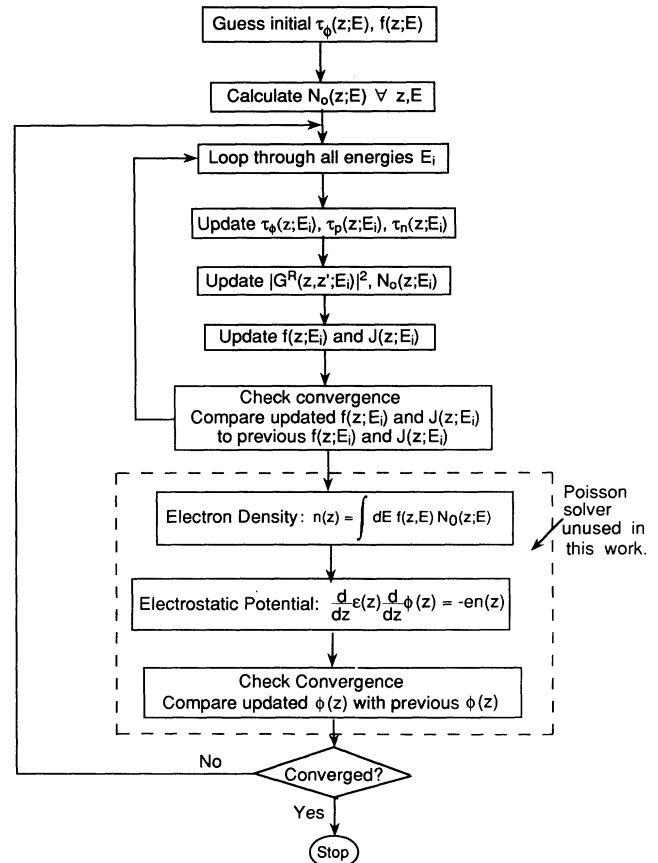


FIG. 12. Flow chart for numerical solution.

and

$$\frac{1}{\langle \tau_\phi(z; E) \rangle} = \frac{1}{\langle \tau_n(z; E) \rangle} + \frac{1}{\langle \tau_p(z; E) \rangle}. \quad (\text{A18})$$

Equations (12)–(15) become Eqs. (A14)–(A18), which are the coupled set of equations that we have numerically solved to provide the results shown in this paper.

The equations for the current density, Eq. (17), and the terminal current, Eq. (23), are treated the same way.

APPENDIX B: SOLUTION PROCEDURE

Figure 12 is a flow chart of the solution procedure when inelastic, energy-dependent scattering is present. To save on notation, all quantities such as the τ 's, N_0 , $|G^R|^2$, and J represent their bracketed counterparts due to averaging over the cross section as described in Appendix A. Note that a Poisson solver for self-consistent electrostatic solutions exists in the loop although it has not been used in the simulations presented in this paper.

APPENDIX C:

FISHER-LEE TRANSMISSION COEFFICIENT

For a strictly 1D (one transverse energy) device, the Fisher-Lee transmission coefficient is⁵⁶

$$T(E) = \hbar^2 v_1 v_2 |G^R(z_1, z_2; E)|^2. \quad (\text{C1})$$

To show that Eq. (25) reduces to (C1) we consider a 1D device with the contact-device interface of contact 1 at point z_1 and the contact-device interface of contact 2 at point z_2 . The contacts are far enough away from the disordered region so that the self-energies are independent of position in the contacts. Then, the Green's function connecting point z in contact 1 and point z' in contact 2 is

$$G^R(z, z'; E) = e^{i\gamma_1(z_1 - z)} G^R(z_1, z_2; E) e^{i\gamma_2(z' - z_2)}, \quad (\text{C2})$$

where

$$\gamma_j = \left[2m^* \left[E - V_j + i \frac{\hbar}{2\tau_{\phi_j}(E)} \right] \right]^{1/2} / \hbar. \quad (\text{C3})$$

In (C3) j stands for either 1 or 2 for γ in contact 1 or 2,

respectively. The integral in (25) becomes

$$\frac{\hbar^2 |G^R(z_1, z_2; E)|^2}{\tau_{\phi_1} \tau_{\phi_2}} \int_{-\infty}^{z_1} dz \int_{z_2}^{\infty} dz' e^{-2\text{Im}\gamma_1(z_1 - z)} \times e^{-2\text{Im}\gamma_2(z' - z_2)}. \quad (\text{C4})$$

Performing the integral in (C4) gives

$$T(E) = \frac{\hbar^2 |G^R(z_1, z_2; E)|^2}{\tau_{\phi_1} \tau_{\phi_2}} \frac{1}{2\text{Im}\gamma_1} \frac{1}{2\text{Im}\gamma_2}. \quad (\text{C5})$$

In terms of E and τ_ϕ ,

$$\text{Im}\gamma = \frac{\sqrt{m}}{\hbar} \left\{ \left[(E - V)^2 + \left(\frac{\hbar}{2\tau_\phi} \right)^2 \right]^{1/2} - (E - V) \right\}^{1/2} \quad (\text{C6a})$$

and

$$\text{Re}\gamma = \frac{\sqrt{m}}{\hbar} \left\{ \left[(E - V)^2 + \left(\frac{\hbar}{2\tau_\phi} \right)^2 \right]^{1/2} + E - V \right\}^{1/2}. \quad (\text{C6b})$$

If we follow Khondker and Alam⁷⁵ and define the group velocity $v(E)$ as

$$v(E) = \frac{\hbar \text{Re}\gamma}{m^*},$$

we evaluate $\text{Im}\gamma$ by multiplying by $v(E)/v(E)$, expanding out all the quantities using (C6), and find

$$\text{Im}\gamma = \frac{1}{2v\tau_\phi}. \quad (\text{C7})$$

If $(E - V) \gg \hbar/2\tau_\phi$, $v(E)$ reduces to the usual quantity $v = [2m(E - V)]^{1/2}/m^*$. Thus the coherent component of the current is given by the usual tunneling formula (26) with the Fisher-Lee form for the transmission coefficient. This result can be extended to multiterminal devices with discrete or continuous transverse modes in each lead. For devices very short compared to L_ϕ , the coherent current is essentially the total current and our quantum kinetic equation reduces to the tunneling formula (26).

¹F. Capasso, K. Mohammed, and A. Y. Cho, IEEE J. Quantum Electron. **QE-22**, 1853 (1986).
²F. Beltram, F. Capasso, D. L. Sivco, A. L. Hutchinson, S. G. Chu, and A. Y. Cho, Phys. Rev. Lett. **64**, 3167 (1990).
³Serge Luryi, in *Heterojunction Band Discontinuities Physics and Device Applications*, edited by Federico Capasso and Giorgio Margaritondo (North-Holland, New York, 1987), p. 489.
⁴M. S. Skolnick, D. G. Hayes, P. E. Simmonds, A. W. Higgs, G. W. Smith, H. J. Hutchinson, C. R. Whitehouse, L. Eaves, M. Henini, O. H. Hughes, M. L. Leadbeater, and D. P. Halliday, Phys. Rev. B **41**, 10754 (1990).
⁵F. Chevoir and B. Vinter, Surf. Sci. **229**, 158 (1990).
⁶A. D. Stone and P. A. Lee, Phys. Rev. Lett. **54**, 1196 (1985).
⁷M. Büttiker, IBM J. Res. Devel. **32**, 63 (1988).
⁸L. I. Glazman and R. I. Shekhter, Zh. Eksp. Teor. Fiz. **94**, 292

(1988) [Sov. Phys. JETP **67**, 163 (1988)].

⁹W. Cai, T. F. Zheng, P. Hu, B. Yudanin, and M. Lax, Phys. Rev. Lett. **63**, 418 (1989).
¹⁰N. S. Wingreen, K. W. Jacobsen, and J. W. Wilkins, Phys. Rev. Lett. **61**, 1396 (1988).
¹¹G. Y. Wu and T. C. McGill, Phys. Rev. B **40**, 9969 (1989).
¹²M. Jonson, Phys. Rev. B **39**, 5924 (1989).
¹³F. Chevoir and B. Vinter, Appl. Phys. Lett. **55**, 1859 (1989).
¹⁴B. Y. Gu, C. Coluzza, M. Mangiantini, and A. Frova, Superlatt. Microstruct. **7**, 29 (1990).
¹⁵V. Pevzner, F. Sols, and Karl Hess, in *Granular Nanoelectronics*, edited by D. K. Ferry, J. R. Barker, and C. Jacoboni (Plenum, New York, 1991), p. 223.
¹⁶F. Sols, Ann. Phys. (to be published).
¹⁷U. Ravaioli, M. A. Osman, W. Potz, N. Kluksdahl, and D. K.

- Ferry, *Physica B* **134**, 36 (1985).
- ¹⁸W. R. Frensley, *Phys. Rev. B* **36**, 1570 (1987).
- ¹⁹N. C. Kluksdahl, A. M. Krivan, D. K. Ferry, and C. Ringhofer, *Phys. Rev. B* **39**, 7720 (1989).
- ²⁰W. R. Frensley, *Rev. Mod. Phys.* **62**, 745 (1990).
- ²¹F. A. Buot and K. L. Jensen, *Phys. Rev. B* **42**, 9429 (1990).
- ²²L. P. Kadanoff and G. Baym, *Quantum Statistical Mechanics* (Benjamin, Reading, MA, 1962).
- ²³L. V. Keldysh, *Zh. Eksp. Teor. Fiz.* **47**, 1515 (1964) [*Sov. Phys. JETP* **20**, 1018 (1965)].
- ²⁴We use 1D to mean devices with one interesting direction and translational invariance in the transverse directions. We will use "strictly 1D" to describe a device with only one quantized transverse energy below the Fermi level.
- ²⁵Antti-Pekka Jauho, *Solid-State Electron.* **32**, 1265 (1989).
- ²⁶P. Danielewicz, *Ann. Phys. (N.Y.)* **152**, 239 (1984).
- ²⁷J. Rammer and H. Smith, *Rev. Mod. Phys.* **58**, 323 (1986).
- ²⁸G. D. Mahan, *Phys. Rep.* **145**, 251 (1987).
- ²⁹S. Datta, *J. Phys. Condens. Matter* **2**, 8023 (1990).
- ³⁰F. S. Khan, J. H. Davies, and J. W. Wilkins, *Phys. Rev. B* **36**, 2578 (1987).
- ³¹K. L. Jensen and F. A. Buot, *Phys. Rev. Lett.* **66**, 1078 (1991).
- ³²G. D. Mahan, *Many-Particle Physics* (Plenum, New York, 1986).
- ³³M. J. McLennan, Y. Lee, and S. Datta, *Phys. Rev. B* **43**, 13 846 (1991).
- ³⁴M. Cahay, M. McLennan, S. Datta, and M. S. Lundstrom, *Appl. Phys. Lett.* **50**, 612 (1987).
- ³⁵F. Sols, M. Macucci, U. Ravaioli, and K. Hess, *J. Appl. Phys.* **66**, 3892 (1989).
- ³⁶A. D. Stone and A. Szafer, *IBM J. Res. Devel.* **32**, 384 (1988).
- ³⁷H. U. Baranger and A. D. Stone, *Phys. Rev. B* **40**, 8169 (1989).
- ³⁸S. Selberherr, *Analysis and Simulation of Semiconductor Devices* (Springer-Verlag, New York, 1984).
- ³⁹M. S. Lundstrom, in *Fundamentals of Carrier Transport: Vol. 10 in the Modular Series on Solid State Devices*, edited by Gerold W. Neudeck and Robert F. Pierret (Addison-Wesley, Reading, MA, 1990).
- ⁴⁰C. B. Duke, *Tunneling in Solids* (Academic, New York, 1969).
- ⁴¹R. Tsu and L. Esaki, *Appl. Phys. Lett.* **22**, 562 (1973).
- ⁴²R. Landauer, *Z. Phys. B* **68**, 217 (1987).
- ⁴³M. Büttiker, *Phys. Rev. Lett.* **57**, 1761 (1986).
- ⁴⁴D. Landheer and G. C. Aers, *Superlatt. Microstruct.* **7**, 17 (1990).
- ⁴⁵M. J. McLennan and S. Datta (unpublished).
- ⁴⁶M. J. McLennan, Master's thesis, Purdue University, 1987 (unpublished).
- ⁴⁷R. Landauer, *Philos. Mag.* **21**, 863 (1970).
- ⁴⁸M. Büttiker, Y. Imry, R. Landauer, and S. Pinhas, *Phys. Rev. B* **31**, 6207 (1985).
- ⁴⁹Y. Imry, in *Directions in Condensed Matter Physics*, edited by G. Grinstein and G. Mazenko (World Scientific, Singapore, 1986), p. 101.
- ⁵⁰R. Landauer, *IBM J. Res. Devel.* **32**, 306 (1988).
- ⁵¹R. Landauer, *IBM J. Res. Devel.* **1**, 223 (1957).
- ⁵²M. Büttiker, *IBM J. Res. Devel.* **32**, 317 (1988).
- ⁵³C. W. J. Beenakker and H. van Houten, in *Solid State Physics*, edited by H. Ehrenreich and D. Turnbull (Academic, New York, 1991), Vol. 44.
- ⁵⁴Equation (23) is obtained using (C5) and (B18) of Ref. 29 and the equilibrium relation (20).
- ⁵⁵G. Neofotistos, R. Lake, and S. Datta, *Phys. Rev. B* **43**, 2442 (1991).
- ⁵⁶D. S. Fisher and P. A. Lee, *Phys. Rev. B* **23**, 6851 (1981).
- ⁵⁷Arthur C. Smith, James F. Janak, and Richard B. Adler, *Electronic Conduction in Solids* (McGraw-Hill, New York, 1967).
- ⁵⁸Since we are working with three-dimensional devices, the resonant level fills up with states of increasing transverse energy. By "bottom of the resonance" we mean the resonant energy of electrons with zero transverse energy.
- ⁵⁹S. Luryi, *Appl. Phys. Lett.* **47**, 491 (1985).
- ⁶⁰S. Luryi, *Superlatt. Microstruct.* **5**, 375 (1989).
- ⁶¹T. Weil and B. Vinter, *Appl. Phys. Lett.* **50**, 1281 (1987).
- ⁶²C. H. Yang, Jean M. Carlson-Swindle, S. A. Lyon, and J. M. Worlock, *Phys. Rev. Lett.* **55**, 2359 (1985).
- ⁶³K. Hess, *Physics of Nonlinear Transport in Semiconductors*, edited D. K. Ferry, J. Barker, and C. Jacoboni (Plenum, New York, 1980), p. 1.
- ⁶⁴R. Landauer, in *Localization, Interaction, and Transport Phenomena*, edited by B. Kramer, G. Bermann, and Y. Bruynseraede (Springer-Verlag, New York, 1985), p. 38.
- ⁶⁵M. Jonson and A. Grincwajg, *Appl. Phys. Lett.* **51**, 1729 (1987).
- ⁶⁶B. G. R. Rudberg, *Semicond. Sci. Technol.* **5**, 328 (1990).
- ⁶⁷Antti-Pekka Jauho, *Phys. Rev. B* **41**, 12 327 (1990).
- ⁶⁸P. Hyltdgaard and A. P. Jauho, *J. Phys. Condens. Matter* **2**, 8725 (1990).
- ⁶⁹E. V. Anda and F. Flores, *J. Phys. Condens. Matter* **3**, 9087 (1991).
- ⁷⁰J. A. Stovng, E. H. Hauge, P. Lipavsky, and V. Spicka, *Phys. Rev. B* **44**, 13 595 (1991).
- ⁷¹X. Wu and S. E. Ulloa, *Phys. Rev. B* **44**, 13 148 (1991).
- ⁷²J. W. Gadzuk, *Phys. Rev. B* **44**, 13 446 (1991).
- ⁷³S. Datta, M. S. Lundstrom, A. Das, R. Lake, M. J. McLennan, and M. Stettler (unpublished).
- ⁷⁴P. M. Morse and H. Feshbach, *Methods of Theoretical Physics* (McGraw-Hill, New York, 1953), p. 884.
- ⁷⁵A. N. Khondker and M. A. Alam, *Phys. Rev. B* **44**, 5444 (1991).

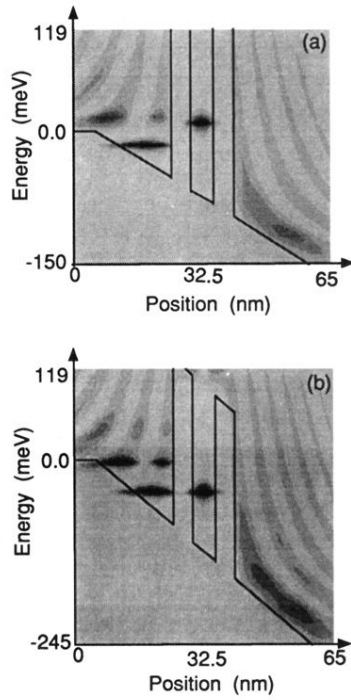


FIG. 9. Shadow plots of the calculated, strictly 1D density of states $N_0(z; E)$, with conduction-band profile superposed corresponding to (a) the first current peak, 150 mV, and (b) the second current peak, 245 mV of Fig. 10. Dark regions are regions of high density of states. The contribution to the density of states from the transverse energies have been ignored in the plot for clarity.